Structural Model Analysis for the Laser Guided Mobile Short-Range Air Defence System

Rimantas BARAUSKAS, Algimantas FEDARAVIČIUS,
Karolis JASAS[*]

Kaunas University of Technology,
50 Studentų Str., 51368, Kaunas, Lithuania
[*]*Corresponding author's e-mail address and ORCID*:
karolis.jasas@ktu.edu; https://orcid.org/0000-0002-7038-5570

Abstract. This article provides structural model analysis of characteristics of the vehicle movement during the shooting from a laser guided short-range air defence system mounted on it. Every shot causes a recoil, which significantly affects vibration of the vehicle and determines the shortest time duration between each two successive shots. The numerical simulation with MATLAB software enabled us verification of the created structural model and it facilitated the understanding of mechanical phenomena which are the most important for achieving the proper vibrational characteristics of the system. Main modes of the system movements during missile launch and their effect on the launcher and the vehicle were determined.
Keywords: Mobile Short-Range Air Defense System, M-SHORAD, Laser Guided Short-Range Air Defense System

1.　INTRODUCTION

The current geopolitical situation makes us rethink and review the state defence plans. Ensuring high operational properties of ground-based air defence systems against low-flying aircrafts such as helicopters is one of the main objectives. According to the NATO classification, ground-based air defence assets are divided into very short range, short-range, medium-range, and long-range systems [14]. Very short-range air defence systems are the most popular due to their simplicity and low acquisition price. Very short-range air defence systems are Man-portable air-defence (MANPAD) systems and mobile short-range air defence (MSHORAD) systems [1]. The specific feature of MANPAD systems is the shot from soldiers' shoulder, as well as by using a tripod placed on the surface of the ground. The specific feature of MSHORAD is the shot from a vehicle, on which the air defence system is mounted. The successful shooting from the short-range air defence system mainly depends on the personnel's experience and training.

Fig. 1. Mobile short-range air defence system [1]

After firing, the air defence system causes vibrations, which affect the whole structure of the armoured vehicle. Vehicle vibrations have a substantial impact on the mobility safety of the carrier. High vibration amplitudes increase driver and crew fatigue, resulting in hazardous driving conditions. The impact of the vibrations on driving safety during shooting must be analysed, [2]. The primary function of the suspension is to offer the passengers a comfortable ride by insulating them from the unevenness of the road surface, as well as to stabilise the vehicle when it turns, brakes, or accelerates.

Vertical and horizontal elasticity, damping, and friction are the primary elements that influence the driving comfort of a vehicle. As the wheels rise and fall due to uneven road surfaces, the springs quickly act as energy storage devices and, as a result, considerably lower the amount of impact stress sent through the suspension to the vehicle structure. The energy of the impact load is proportional to the product of the applied force and the action-limiting distance of the spring medium. A soft spring of low coefficient of elasticity, that permits a substantial deflection from the average value, will reduce the magnitude of forces conveyed to the occupants of a car. Shooting from a mobile short-range air defence system has an additional impact on the vehicle chassis. This effect intensifies when travelling on the road with undulations, [3, 4, 5].

2. STRUCTURAL MODEL FOR THE ANALYSIS OF VIBRATIONS OF THE MSHORAD SYSTEM

For simulation of mechanical vibrations of the vehicle during the live firings, the structural dynamic model, based on the standard discrete system approach, was developed [6, 7]. The vehicle with the mounted firing system consists of rigid bodies each of which perform planar motion. The rigid bodies are connected by springs representing elasticities of the structural joints, as they are in the real structure. The motion of each body is described by the motion of its mass centre C and the rotation angle α. Spring is attached to the body at the point P, which can be different from the mass centre. Its position, with respect to the mass centre, is described by the distance L and the angle φ. Figure 2 presents a sample body in its standard position, where the mass centre is at the origin of the coordinates and Fig. 3 represents the displaced position of the body.
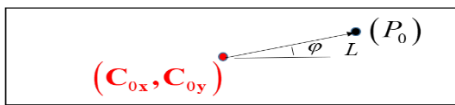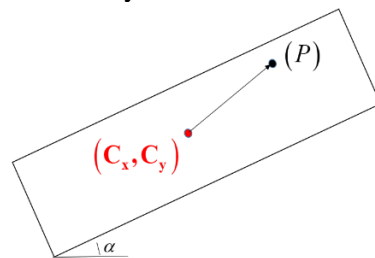
Fig. 2. Standard body position   Fig. 3. Displaced body position

In Figure 2, the vector r_0 from the mass centre to the point P_0 reads as

$$\vec{r}_0 = L \begin{pmatrix} \cos\varphi \\ \sin\varphi \end{pmatrix} \tag{1}$$

In the displaced position (Fig. 3), the vector *r* and the coordinates of the point *P* read as

$$\vec{r} = L \begin{bmatrix} \cos\alpha & -\sin\alpha \\ \sin\alpha & \cos\alpha \end{bmatrix} \begin{pmatrix} \cos\varphi \\ \sin\varphi \end{pmatrix} \tag{2}$$

$$\left(P_x, P_y\right) = \left(C_x, C_y\right) + \vec{r} \tag{3}$$

The displacement of the point of attachment of the spring is obtained by combining the displacement vector of the centre of mass and the angle of planar rotation about the centre of mass (Fig. 4):

$$\vec{u}_P = \vec{u} + \begin{pmatrix} 0 \\ 0 \\ \theta \end{pmatrix} \times \vec{r} = \vec{u} + \theta \begin{pmatrix} -r_y \\ r_x \end{pmatrix} \tag{4}$$
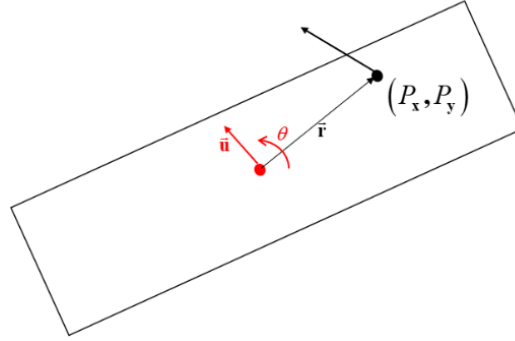

Fig. 4. Kinematics of a planar body

Each pair of bodies in the structure can be mutually connected by a bidirectional mathematical spring. It may exhibit elastic forces in two perpendicular directions corresponding to normal and tangential displacement directions of the points P_1 with respect to the point P_2, Figs. 5 and 6. The two perpendicular directions of the spring are represented by unit vectors as:

$$\vec{n} = \frac{P_2 - P_1}{norm(P_2 - P_1)} \tag{5}$$

$$\vec{\tau} = \begin{pmatrix} -n_y \\ n_x \end{pmatrix} \tag{6}$$

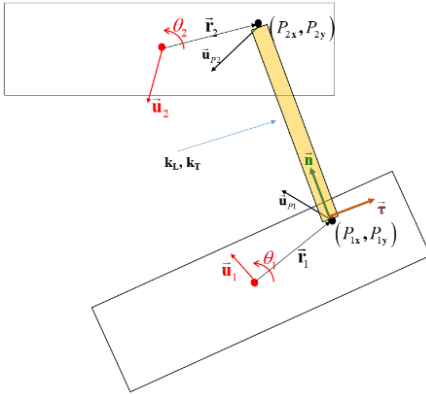The corresponding normal and tangential stiffness coefficients are denoted as k_L, k_T.

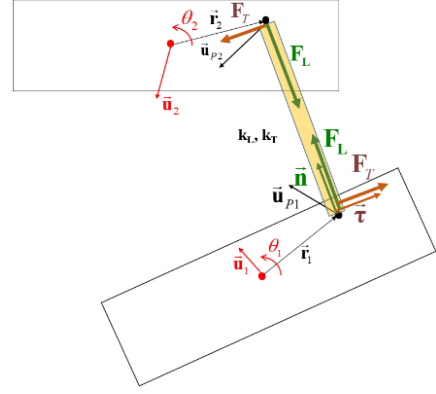Fig. 5. Two-way spring, stiffness coefficients k_L, k_T

Fig. 6. Spring tension forces in two directions

The structural element consists of two planar bodies connected by a bidirectional spring. Here, we show how the elastic forces acting on bodies are calculated. F_L and F_T describe the spring tension force in two directions:

$$\mathbf{F_L} = k_L \left(\mathbf{\bar{u}}_{P2} - \mathbf{\bar{u}}_{P1} \right) \square \mathbf{\bar{n}} \tag{7}$$

$$\mathbf{F}_T = k_T \left(\mathbf{\bar{u}}_{P2} - \mathbf{\bar{u}}_{P1} \right) \square \mathbf{\bar{\tau}} \tag{8}$$

$$\begin{cases} \vdots \\ m_1 \ddot{u}_{1x} = n_x F_L + \tau_x F_T + \cdots \\ m_1 \ddot{u}_{1y} = n_y F_L + \tau_y F_T + \cdots \\ I_1 \ddot{\theta}_1 = \left(\mathbf{\bar{r}}_1 \times \left(F_L \mathbf{\bar{n}} + F_T \mathbf{\bar{\tau}} \right) \right)_z + \ldots \\ \vdots \\ m_2 \ddot{u}_{2x} = -n_x F_L - \tau_x F_T + \cdots \\ m_2 \ddot{u}_{2y} = -n_y F_L - \tau_y F_{Ti} + \cdots \\ I_2 \ddot{\theta}_2 = -\left(\mathbf{\bar{r}}_2 \times \left(F_L \mathbf{\bar{n}} + F_T \mathbf{\bar{\tau}} \right) \right)_z + \ldots \\ \vdots \end{cases} \tag{9}$$

By combining Eqs. (5-9) and assembling the structural equation, we arrive to the structural dynamic equation without damping:

$$\mathbf{M\ddot{U} + KU = 0} \tag{10}$$

In Eq. (10), the structural matrices $\mathbf{K}$ and $\mathbf{M}$ are assembled of element matrices, the formulas of which read as:

The stiffness matrix:

$$K^e = \begin{bmatrix} K_{xx} & K_{xy} & K_{xr1} & -K_{xx} & -K_{xy} & -K_{xr2} \\ K_{xy} & K_{yy} & K_{yr1} & -K_{xy} & -K_{yy} & -K_{yr2} \\ r_{1x}K_{xy}-r_{1y}K_{xx} & r_{1x}K_{yy}-r_{1y}K_{xy} & K_{r11} & -r_{1x}K_{xy}+r_{1y}K_{xx} & -r_{1x}K_{yy}+r_{1y}K_{xy} & -K_{r12} \\ -K_{xx} & -K_{xy} & -K_{xr1} & K_{xx} & K_{xy} & K_{xr2} \\ -K_{xy} & -K_{yy} & -K_{yr1} & K_{xy} & K_{yy} & K_{yr2} \\ -r_{2x}K_{xy}+r_{2y}K_{xx} & -r_{2x}K_{yy}+r_{2y}K_{xy} & -K_{r21} & r_{2x}K_{xy}-r_{2y}K_{xx} & r_{2x}K_{yy}-r_{2y}K_{xy} & K_{r22} \end{bmatrix}, \quad (11)$$

$$K_{xx} = k_L n_x n_x + k_T \tau_x \tau_x$$
$$K_{xy} = k_L n_x n_y + k_T \tau_x \tau_y$$
$$K_{yy} = k_L n_y n_y + k_T \tau_y \tau_y$$
$$K_{xr1} = k_L n_x \left(-r_{1y}n_x + r_{1x}n_y\right) + k_T \tau_x \left(-r_{1y}\tau_x + r_{1x}\tau_y\right)$$
$$K_{yr1} = k_L n_y \left(-r_{1y}n_x + r_{1x}n_y\right) + k_T \tau_y \left(-r_{1y}\tau_x + r_{1x}\tau_y\right)$$
$$K_{xr2} = k_L n_x \left(-r_{2y}n_x + r_{2x}n_y\right) + k_T \tau_x \left(-r_{2y}\tau_x + r_{2x}\tau_y\right) \quad (12)$$
$$K_{yr2} = k_L n_y \left(-r_{2y}n_x + r_{2x}n_y\right) + k_T \tau_y \left(-r_{2y}\tau_x + r_{2x}\tau_y\right)$$
$$K_{r11} = r_{1x}k_L n_y \left(-r_{1y}n_x + r_{1x}n_y\right) + r_{1x}k_T \tau_y \left(-r_{1y}\tau_x + r_{1x}\tau_y\right) - r_{1y}k_L n_x \left(-r_{1y}n_x + r_{1x}n_y\right) - r_{1y}k_T \tau_x \left(-r_{1y}\tau_x + r_{1x}\tau_y\right)$$
$$K_{r12} = r_{1x}k_L n_y \left(-r_{2y}n_x + r_{2x}n_y\right) + r_{1x}k_T \tau_y \left(-r_{2y}\tau_x + r_{2x}\tau_y\right) - r_{1y}k_L n_x \left(-r_{2y}n_x + r_{2x}n_y\right) - r_{1y}k_T \tau_x \left(-r_{2y}\tau_x + r_{2x}\tau_y\right)$$
$$K_{r21} = r_{2x}k_L n_y \left(-r_{1y}n_x + r_{1x}n_y\right) + r_{2x}k_T \tau_y \left(-r_{1y}\tau_x + r_{1x}\tau_y\right) - r_{2y}k_L n_x \left(-r_{1y}n_x + r_{1x}n_y\right) - r_{2y}k_T \tau_x \left(-r_{1y}\tau_x + r_{1x}\tau_y\right)$$
$$K_{r22} = r_{2x}k_L n_y \left(-r_{2y}n_x + r_{2x}n_y\right) + r_{2x}k_T \tau_y \left(-r_{2y}\tau_x + r_{2x}\tau_y\right) - r_{2y}k_L n_x \left(-r_{2y}n_x + r_{2x}n_y\right) - r_{2y}k_T \tau_x \left(-r_{2y}\tau_x + r_{2x}\tau_y\right)$$

The mass matrix:

$$M = \begin{bmatrix} m_1 & & & & & \\ & m_1 & & & & \\ & & I_1 & & & \\ & & & m_2 & & \\ & & & & m_2 & \\ & & & & & I_2 \end{bmatrix} \quad (13)$$

where m_1, I_1, m_2, and I_2 are the masses and mass moments of inertia of two bodies comprising a structural element, and:

$$U^e = \begin{pmatrix} u_{1x} \\ u_{1y} \\ \theta_1 \\ u_{2x} \\ u_{2y} \\ \theta_1 \end{pmatrix} \qquad (14)$$

is the nodal displacement vector of the structural element.

Non-zero solutions of the homogeneous differential equation, whose free terms are zero, are called the solutions. We are looking for natural solutions as:

$$\mathbf{U} = \hat{\mathbf{U}}\cos(\omega t + \varphi) \qquad (15)$$

where ω is the natural vibration frequency, $\hat{\mathbf{U}}$ is the natural vector of nodal amplitudes, and φ is the initial phase of the oscillations.

After inserting Eq. (15) into dynamic Eq. (10), we obtain the system of algebraic equations that have non-zero solutions only if:

$$\det(\mathbf{K} - \omega^2 \mathbf{M}) = 0 \qquad (16)$$

This equation is called the natural value (eigenvalue) problem. The physical meaning of the natural vector are the displacements of the structure harmonically oscillating at the natural frequency at the time moment when they reach their limit values. Each pair $\omega_i, \mathbf{U}^i$ is called the vibration mode of the structure. The number of modes is always equal to the number of degrees of freedom of the structure.

The dynamic equation of free vibrations of the damped (non-conservative) system could be obtained by extending Eq. (10) as

$$\mathbf{M}\ddot{\mathbf{U}} + \mathbf{C}\dot{\mathbf{U}} + \mathbf{K}\mathbf{U} = 0 \qquad (17)$$

where $\mathbf{C}$ is the damping matrix.

Now, two options of analysis are possible. The simplified approach assumes the proportional form of the damping matrix as $\mathbf{C} = \alpha\mathbf{M} + \beta\mathbf{K}$, where α, β are the coefficients the values of which are based on the average decay of transient free vibration amplitudes. In such a case, the modal shapes of non-damped free vibration problem as Eq. (16) can be used as independent coordinates of the damped structure.

In the general case, the damping matrix $\mathbf{C}$ is formed independently of the matrices $\mathbf{M}$ and $\mathbf{K}$ by using the measured damping coefficients in each connection between the rigid bodies comprising the structure. This leads to the complex eigenvalue problem as:

$$\det(\lambda^2 \mathbf{M} + \lambda \mathbf{C} + \mathbf{K}) = 0 \qquad (18)$$

where λ is the complex eigenvalue and it represents both frequency and the decay rate of the free vibration amplitude.

In this work, the research was limited to the analysis of undamped modes of the structure of the MSHORAD system. The solution procedure has been implemented in the MATLAB software by using the eigenvalue solver eig.

2.1 Boundary conditions

A dynamic model of the MSHORAD system is illustrated in Fig. 7. The bidirectional penalty spring c_7 represents a hinge of launcher No. 4. Bidirectional springs represent the tires and hangers, tires marked 5 and 6, hangers 1 and 2 which are strengthen easily.
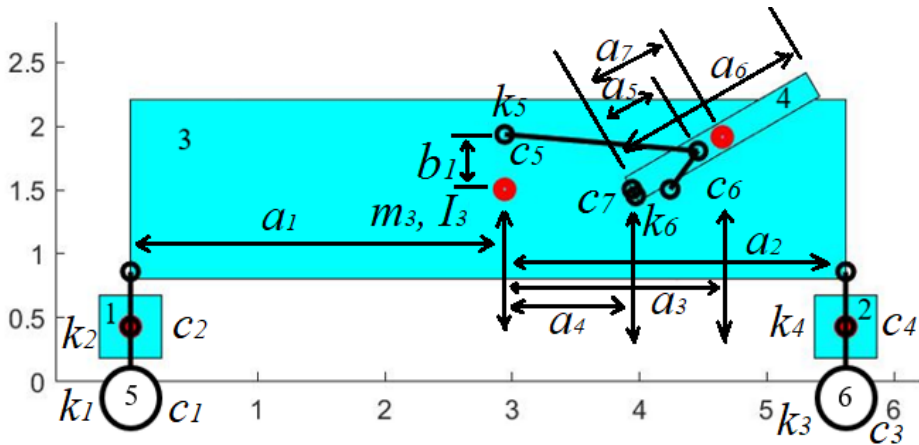

Fig. 7. Dynamic model

The structure consists of 4 rigid bodies each of which has 3dof (two displacements and one rotation). However, from the total number of 12dof, only 8dof are active in the model as the wheels are not allowed neither to rotate nor to move horizontally. Only up-down vibrations of the wheels are possible because of the elasticity of the tires and the suspension. The hinge between vehicle body 3 and launcher 4 is represented by 2 nodes on each of bodies 3 and 4 connected together by the bidirectional penalty spring. The stiffness of the penalty spring is chosen much higher than all other stiffnesses in the structure in order to prevent any appreciable displacement in the hinge.

Table 1 shows the values of the quantitative data as stiffnesses of springs and damping coefficients of dampers which are necessary for the final implementation of the model.

Table 1. Input parameters in the dynamic process model [8, 9, 10]

Parameter	Value	Parameter	Value	Parameter	Value	Parameter	Value
K_1 [kN/m]	800000	C_4 [kN s/m]	54000	a_2 [m]	2.68	m_1 [kg]	775
C_1 [kN s/m]	250	K_5 [kN/m]	6000000	a_3 [m]	1.3	m_2 [kg]	1550
K_2 [kN/m]	600000	C_5 [kN s/m]	300000	a_4 [m]	1	m_3 [kg]	3800
C_2 [kN s/m]	11000	K_6 [kN/m]	6000000	a_5 [m]	0.6	m_4 [kg]	80
K_3 [kN/m]	6000000	C_6 [kN s/m]	300000	a_6 [m]	1.64	I_3 [kg m^3]	45591
C_3 [kN s/m]	700	C_7 [kN s/m]	2e10	a_7 [m]	0.82	I_4 [kg m^3]	895
K_4 [kN/m]	1122000	a_1 [m]	2.94	b_1 [m]	0.43	α_0	$\pi/6$

The structural model which represents the missile launch from the mobile short-range air defence system RBS-70 has been developed (Fig. 2). The model illustrates the first stage of the missile launch motion. The mass centre of the vehicle is marked – c_3. The physical model describes the interaction between the air defence system and the vehicle with mechanical springs with elastic springs k_1, k_2, k_3, k_4, k_5, k_6 and the dampers c_1, c_2, c_3, c_4, c_5, c_6. The recoil force of air defence systems is F [11,12,13]. The launcher is hinged to the vehicle body. In the model, the stiffness of the hinge is represented by the penalty stiffness k_7.

3. ANALYSIS OF RESULTS

The dynamic properties in the MSHORAD system structural model were analysed using the MATLAB software. The main result of this research was the obtained vibration modes of the system.

The availability of the damping coefficients in the joints of the structure principally enables us to form a full non-conservative model. However, in this study, the simplification was used by assuming proportional damping as explained in section 2. In case of proportional damping, the modal shapes of an undamped system may be used as independent coordinates and they may be regarded as the most important characteristics of the structure.

Further, we present the modes of vibration obtained by using the structural model. The structure has 8dof, however, we present only 6 the lower modes. The remaining two higher modes are caused by the elasticity of the penalty spring in two perpendicular directions. Their vibration frequencies are determined by penalty stiffness and they are far above the range of the engineering importance.

The modes describe the harmonic vibration in which all bodies of the structure move at the same frequency and the same phase. The graphical representation of the modes illustrates the deformed shape of the structure as its displacements are at the maximum of their absolute values.

The results of the first 6 modal shapes and modal frequencies are provided in Table 2, as well as they are illustrated in Figs. 8-13. Norming multipliers for modal shapes are chosen such that $\mathbf{y}_i^T \mathbf{M} \mathbf{y}_i = 1$, where y_i is the vector-column of the i-th modal shape and $\mathbf{M}$ is the mass matrix of the structure.

Table 2. The results of the first 6 modal shapes and modal frequencies

Mode number	1	2	3	4	5	6
Modal frequency (Hz)	2.19576	2.67647	7.98915	8.43164	9.89058	19.3241
Displacement *y* of rear wheel	-0.0006	-0.0155	0.0023	0.0026	-0.0017	0.0322
Displacement *y* of front wheel	0.0130	-0.0031	-0.0034	-0.0028	0.0212	0.0004
Displacements *x, y* of mass centre and rotation angle of vehicle body	-0.0023	-0.0022	-0.0151	-0.0040	-0.0019	0.0002
	0.0084	-0.0108	0.0007	0.0011	-0.0063	-0.0055
	0.0031	0.0027	-0.0005	-0.0004	-0.0017	0.0013
Displacements *x, y* of mass centre and rotation angle of launcher	-0.0012	-0.0011	-0.0190	0.0104	-0.0011	-0.0001
	0.0098	-0.0098	0.0060	-0.0205	-0.0091	-0.0038
	-0.0024	-0.0025	0.0085	-0.0311	-0.0016	0.0006
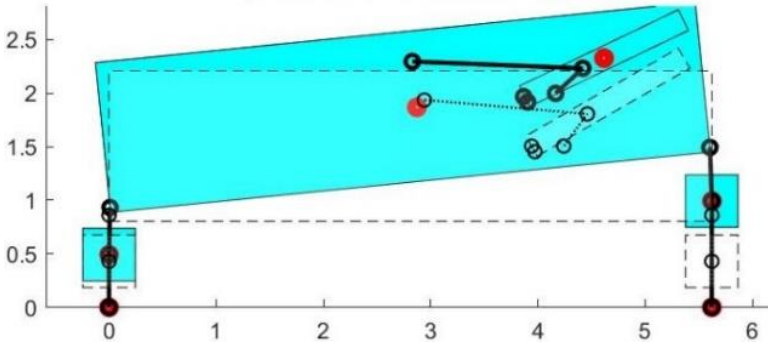
Fig. 8. Mode No. 1, frequency $f = 2.19576$ Hz
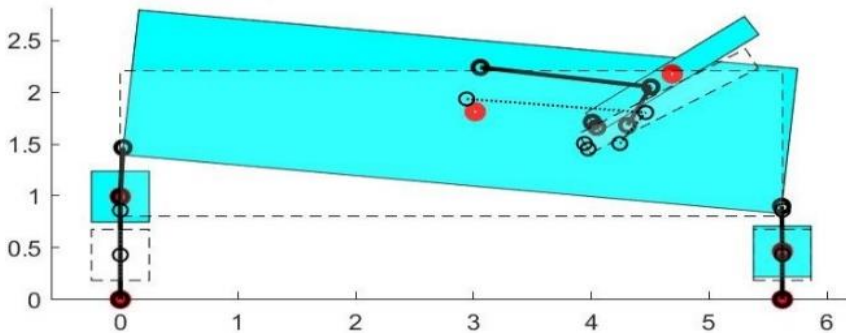
Fig. 9. Mode No. 2 , frequency $f = 2.67647$ Hz

Figure 8 describes mode No. 1 vibration when it reaches maximum displacement which is $f = 2.19576$ Hz. Figure 9 describes mode No. 2 vibration when it reaches maximum displacement which is $f = 2.67647$ Hz
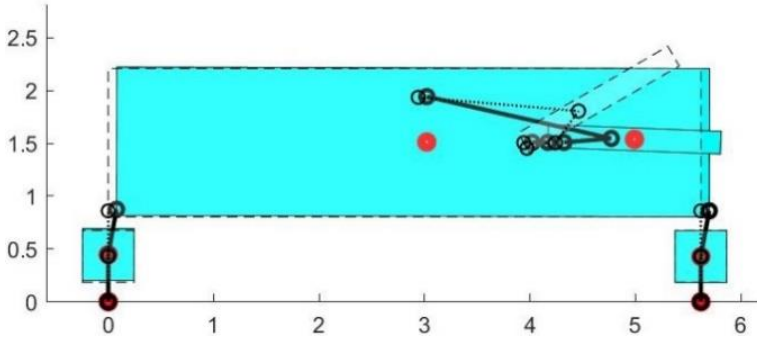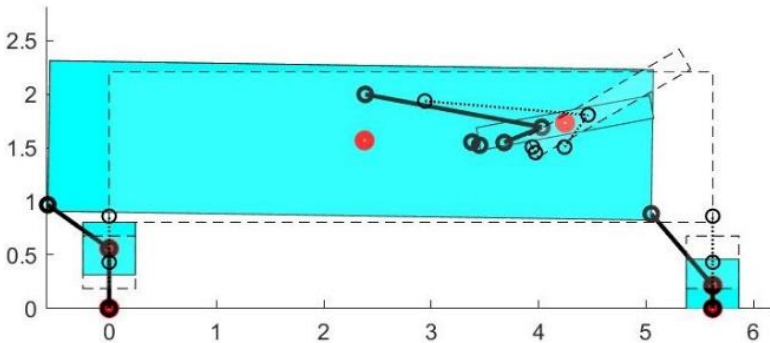

Fig. 10. Mode No. 3 , frequency $f = 7.98915$ Hz

Fig. 11. Mode No. 4 , frequency $f = 8.43164$ Hz

Figure 10 describes mode No. 3 vibration when it reaches maximum amplitude which is $f = 7.98915$ Hz. Figure 11 describes mode No. 4 vibration when it reaches maximum amplitude which is $f = 8.43164$ Hz

Figure 12 describes mode No. 5 vibration when it reaches maximum displacement, $f = 9.89058$ Hz. Figure 13 describes mode No. 6 vibration when it reaches maximum displacement, $f = 19.3241$ Hz
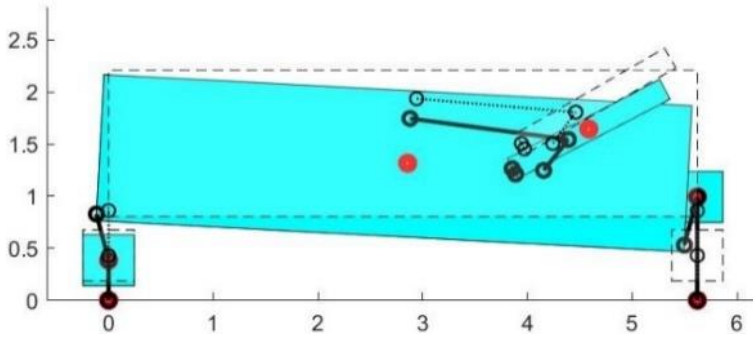
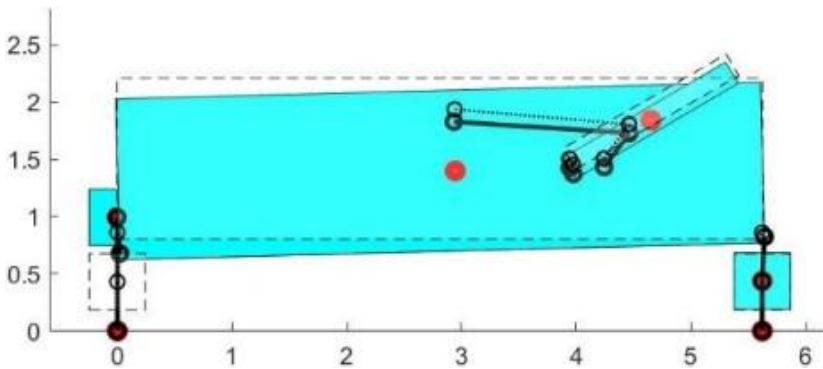Fig. 12. Mode No. 5 , frequency f = 9.89058 Hz

Fig. 13. Mode No. 6 , frequency f = 19.3241 Hz

4.   CONCLUSIONS

In this work, the first stage of the launch of the short-range air defence system RBS-70 missiles was analysed. After theoretical research, the structural model of the first stage of the launch of the short-range air defence system missiles was developed.

Computer modelling and analysis of physical phenomena have been performed, considering the analytical dependence related to the system motion. The system movements during missile launch and their effect on the launcher were determined according to the initial system parameters.

The model has been developed by using simplifications, such as small vibration amplitudes and proportional damping. Therefore, the research will be continued in order to find the vibration modes of the non-conservative system, where both modal shapes and frequencies are expressed in terms of complex numbers.

This will be done by using non-proportional damping matrix, where the measured damping coefficients are employed for obtaining the damping matrix, and for solving the complex eigenvalue problem. The chosen approach of the standard discrete system for building the dynamic model allows us easy transition to transient vibration analysis, as well as, to large displacement vibrations of the system.

FUNDING

REFERENCES

[1] Army Recognition, Defense News. March 2022. *Global Security army industry, Saab reveals finalized MSHORAD air defense system*. Available from:https://www.armyrecognition.com/defense_news_march_2022_global_security_army_industry/saab_reveals_finalized_mshorad_air_defense_system.html [accessed 12 April 2022].

[2] Priegnitz, J. 1999. "Future armoured and non-armoured vehicles in the German army". *Military Technology* 23 (2) : 43-49.

[3] Popp, Karl, and Werner Schiehlen. 2010. *Ground Vehicles Dynamics*. Springer.

[4] Sapragonas J., and Rolandas Makaras. 2011. "Investigation of movement of the off-road vehicles under roadless conditions". *Journal of Vibroengineering* 13 (3) : 334-341.

[5] Jazar, N. Reza. 2008. *Vehicle Dynamics: Theory and Application*. Springer.

[6] Barauskas, Rimantas, and R. Barauskienė. 2011. *Physical Behavior Animations: Rigid Body Systems,* ISBN: 978-9955-25-936-7.

[7] Žiliukas A., and Rimantas Barauskas. 1997. *Mechanical Vibrations* (in Lithuanian), ISBN: 978-9955-20-275-2.

[8] Fedaravičius, Algimantas, Karolis Jasas, Egidijus Sližys, and Arvydas Survila. 2022. "Modelling of the Missile Launch Dynamic Processes in Short range air defense system". *Mechanika* 28 (1) : 32-37.

[9] Dugalic, Adnan. 2018. "NG stand mechanical interface analysis for vehicle integrated RBS 70 NG". Available from Internet: http://www.diva-potal.org/sma sh/get/diva2:1236120/FULLTEXT02.pdf. [accessed 1 May 2022].

[10] Abdelkareem, AA Mohamed, Mostafa M Makrahy, Ali M Abd-El-Tawwab, Asa El-Razaz, Mohamed Kamal Ahmed Ali, and MM Moheyeldein. 2018. "An analytical study of the performance indices of articulated truck semi-trailer during three different cases to improve the driver comfort". *Proceedings of the Institution of Mechanical Engineers. Part K, Journal of multi-body dynamics* 232 (1) : 84-102.

[11] Sandor, Bela Imre. 1987. *Engineering Mechanics Statics and Dynamics*. 2nd ed., Prentice Hall, Inc., Englewood Cliffs, N. J.

[12] Bogdevičius, M., R. Junevičius, and V. Vansauskas. 2012. *Vehicle dynamics*, ISBN: 978-609-457-276-0.

[13] Fedaravičius, Algimantas, Vaclovas Jonevičius, Arvydas Survila, and Albertas Pincevičius. 2013. "Dynamics study of the carrier HMMWV M1151". *Journal of Vibroengineering, Vibromechanika* 15 (3) : 1619-1626.

[14] Joint Warfare Publication 3-63 (JWP 3-63), is promulgated. The Joint Doctrine & Concepts Centre MoD. Posted on July 2003. Available from: https://assets.publishing.service.gov.uk/government/uploads/system/upload s/attachment_data/file/784305/archive_doctrine_uk_joint_air_defence_jwp _3_63.pdf . [accessed 12 September 2022].